Interaction of Diatom Silica with Graphene

Juliet Q. Dalagan[1,2]* and Erwin P. Enriquez[2]

[1] Chemistry Department, Xavier University-Ateneo de Cagayan, Corrales Avenue, Cagayan de Oro City, 9000
[2] Department of Chemistry, Ateneo de Manila University, Loyola Heights, Quezon City, 1108

In this present work, the synthesis and characterization of graphene-diatom silica were studied. Diatom silica-graphene composite was prepared via the adsorption of graphene suspension into diatom silica extracted from 3 different species, namely *Amphora sp., Navicula ramossisira* and *Skeletonema sp.* The adsorption proceeded to yield a black solid material that is composed of silica and graphene. The concentrations of graphene in the 3 diatom species based on thermogravimetric and UV-Vis spectroscopic methods were 0.306 mg/mL, 0.449 mg/mL and 0.188 mg/mL for *Amphora sp., Navicula ramossisira* and *Skeletonema sp*., respectively. Raman spectroscopy of the graphene-diatom silica revealed band shifts in the D, G and 2D peaks which are indicative of an interaction between graphene and diatom silica. Scanning Electron Microscopic (SEM) images also illustrate presence of graphene on diatom silica.

KEYWORDS

biogenic silica; composite; diatom; diatomites; graphene

*Corresponding author
Email Address: j.dalagan@xu.edu.ph
Received: October 14, 2012
Revised: May 10, 2013
Accepted: May 21, 2013
Published: June 21, 2013
Editor-in-charge: Gisela P. Padilla - Concepcion

INTRODUCTION

Graphene, a 2-D single layer of carbon densely packed in a benzene ring structure, is a fast rising star in the field of materials science due to its unique and interesting properties. It has very high mechanical stiffness and strength, high and tunable electrical and thermal conductivity (Allen et al. 2010). Recently, graphene-based composite materials have gained popularity in the scientific community because of their wide variety of possible uses. Silica-carbon composites have been prepared using chemically derived silica from a silica precursor, tetraethoxyorthosilicate (TEOS) (Kawashima et al. 2000; Hubert et al. 2005; Grzelczak et al. 2006; Wang et al. 2006; Chu et al. 2007; Wan et al. 2008; Song et al. 2010). Chu et al. (2005) used a mechanochemical intercalation approach to introduce TEOS into surfactant-preexpanded graphite oxide. The silica structure in the composite was altered from a disordered structure to a condensed silica network when the amount of TEOS was increased. The porosity formation was greatly affected by the increase in silicon content. Silica-graphene composite prepared by Watcharotone et al. (2007) via sol-gel method exhibited enhanced electrical properties. Wang et al. (2010) developed a method to synthesize metal oxide-graphene nanocomposites using surfactant or polymer directed self-assembly approach with SiO_2, NiO, SnO_2 and MnO_2 as the metal oxides. Results revealed that ternary self-assembly approach constructed an ordered metal oxide-graphene nanocomposites which have high surface area and contain conductive networks. These materials find application as electrode for electrochemical energy storage devices. The silica material used in the studies mentioned above was synthetically produced. A material of significant interest to combine with graphene is silica from a natural source, the

diatom. Diatoms are microscopic, photosynthetic unicellular algae that thrive in both marine and freshwater environment. One of its interesting properties is the extraordinary capability to produce an amorphous silica shell or frustules which are nanoporous. Each diatom species expresses a variety of intricate and unique architecture of biosilica cell wall. To the author's knowledge, graphene – diatom silica composites have not yet been reported. However, composite material from diatomites (silica from fossilized diatoms) and carbon nanotubes (CNT) was prepared by Yu and Fugetsu (2010) by the adsorption of CNT into the pores of the diatomites. Agglomerates of CNT were dispersed using an anionic surfactant, sodium n-dodecyl itaconate and the resulting dispersed CNTs were inserted into cavities of diatomites to form the composite of diatomite/CNT. The composite was made into an adsorbent for organic dyes and results showed that it has the highest adsorption capacity compared with diatomite or CNT alone.

Exploiting the intricate design and intriguing optical, physical, surface and mechanical properties of silica extracted from three diatom species (De Stefano et al., 2009) made the preparation of a diatom silica-graphene composite new and challenging. Herein, we report the preparation and characterization of diatom silica-graphene composites using 3 different diatom species. *Amphora sp*. is a common benthic marine pennate diatom. *Navicula ramossisira* is also a pennate diatom with boat-shaped cells that may exist singly or in ribbons (Cooksey B and Cooksey K, 2005). *Skeletonema sp*. is a centric diatom that grows primarily in marine and estuaries (Spaulding, 2009). Specific surface area of diatoms ranges from 10-300 m^2/g (Vrieling et al. (1999).

MATERIALS AND METHODS

Isolation and characterization of diatom silica, graphene and diatom silica-graphene composite

The three diatom species used in this study (*Navicula ramossisima*, *Amphora sp*., and *Skeletonema sp*.) were obtained from the Southeast Asian Fisheries Development Center Aquaculture department (SEAFDEC-AQD), Tigbauan, Iloilo City and cultured using Guillards F2 medium at 25 ˚C. Diatoms were harvested after 7 days of culturing and cleaned as previously described (Bismuto et al. 2008). Fifty (50) mL of concentrated diatom sample was centrifuged (Sorvall Legend RT centrifuge) at 4600 rpm for 30 min followed by 5 times washing of the pellet with distilled water. For full removal of the organic matrix covering the siliceous frustules, excess concentrated sulfuric acid was used. The solution turned green after adding concentrated sulfuric acid. The acid was removed and solution turned grayish white indicating removal of organic components in diatom. The biosilica pellet was washed again 5 times with distilled water and ethanol. Biosilica pellets were oven dried and followed by vacuum drying. Dried biosilica was stored in a desiccator.

After the diatoms were harvested and cleaned, optical images were taken using the Olympus Tokyo. Presence of the different functional groups such as silanol and siloxane in diatom silica was monitored using IR Affinity-1 FTIR Shimadzu instrument using the KBr pellet standard method and scanned at 4 cm-1 resolution. Morphology was observed using scanning electron microscopy (SEM). The samples were placed on aluminum substrate and mounted on the stage with a conducting tape and imaged using a Hitachi TM-1000 Tabletop Microscope. The accelerating voltage and emission current used were 15 kV and 70 mA, respectively.

All diatom samples were characterized by powder Xray diffraction using a Bruker Davinci Diffractometer (Cu Kα radiation = λ = 1.5418 A). Nitrogen adsorption/desorption of diatom silica was performed with a Micromeritics ASAP 2010 Analyzer (Micromeritics Instrument Corporation, Norcross, GA). The samples were outgassed under vacuum and 150˚C for 24 h prior to analysis.

Graphene was prepared via liquid exfoliation method reported by Hernandez et al (2008). Graphite (Ansac Sendirian Berhad) was added with N-methyl pyrolidinone (NMP) and sonicated for 3 hours followed by centrifugation at 4600 rpm for 1 h at 30 ˚C. The supernatant liquid was centrifuged at 4600 rpm for 30 min at 30 ˚C and the supernatant liquid which contains exfoliated graphene was collected. The graphene suspension was observed to be stable even after two months, showing no flocculation of the suspended graphene.

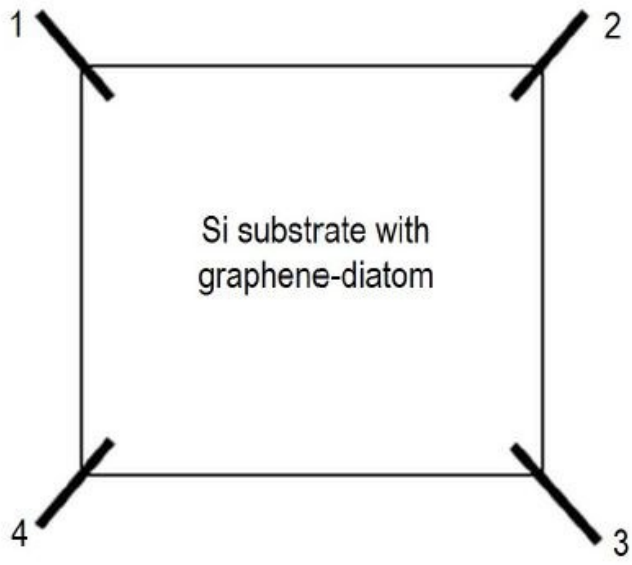

Figure1. Schematic diagram of sample in Hall mobility measurement where the four leads (wires) are connected to the four ohmic contacts on the edges of the sample

The graphene dispersion was deposited on piranha-cleaned silicon wafer substrate and dried with nitrogen. Atomic Force Microscopy (Veeco Dimension Icon)-tapping mode in air was used to investigate the topography of the exfoliated graphene and Raman spectra were collected using NT-MDT NTEGRA with an excitation wavelength of 473 nm at room temperature.

The diatom silica-graphene composite was characterized by SEM, FTIR, Raman and Hall measurement. Hall electron mobility was measured using the Hall instrument. Sample was drop casted on Si wafer substrate and dried in air. The resistance of the film was checked with a multimeter prior to Hall measurement. The sample was placed in the sample chamber where four leads (wires) are connected to the four ohmic contacts of the sample (see Figure 1). The measurement was carried out in the presence of a magnetic field where a positive magnetic field was applied first followed by the reversed field.

The amount of graphene in diatom silica was determined by thermogravimetric analysis. It was carried out using a Shimadzu TGA- 50 interfaced with Shimadzu TA-501 Thermal Analyzer. Samples (16-20 mg) were loaded into platinum crucible and heated under a flow of nitrogen (20 mL/min) from room temperature to 600 ˚C at a rate of 20 ˚C/min and a hold time of 10 minutes. It was further heated to 800 ˚C at a rate of 10 ˚C/min in air. The constant mass of the sample after all the graphene has combusted at 800 ˚C indicates the mass of silica. The concentration of graphene was then determined as mg graphene in 100 μL of the graphene suspension.

Equilibration of graphene with diatom silica

One milligram of biosilica was equilibrated with 5 ml of graphene dispersion of different dilution (20x, 10x, 5x, and 3x) for 24 hrs at 150 rpm at 30 ˚C using the Thermal Incubating Shaker. Graphene without silica served as control sample and it was equilibrated alongside with graphene-diatom silica. The resulting suspension was centrifuged at 4600 rpm for 20 min at 30 ˚C. The precipitate was stored for partial characterization and the supernatant liquid was analyzed for the presence of graphene using the Shimadzu UV2401-PC UV-Vis spectrophotometer. Quartz cuvettes were used and the blank reference was the NMP solvent.

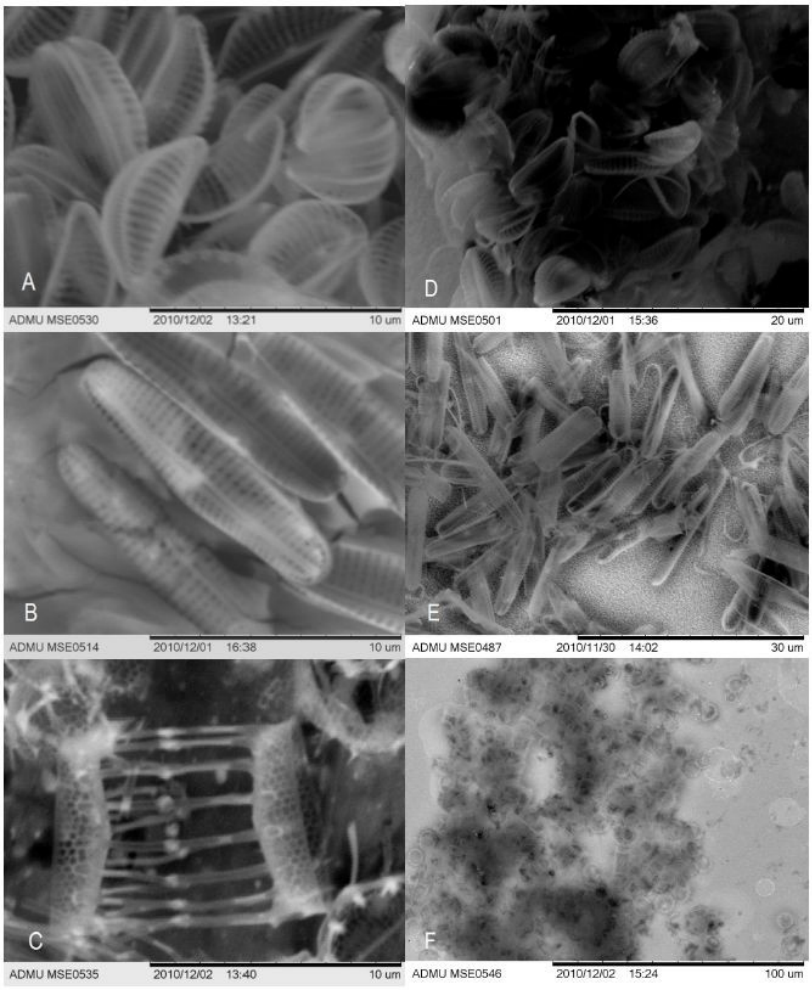

Figure 2. (A-C) SEM images of diatoms (A) *Amphora sp*., (B) *Navicula ramossisima*, and (C) *Skeletonema sp*. ; (D-F) SEM of diatom silica with graphene (A. *Amphora*-graphene, B. *navicula*-graphene, C. *Skeletonema*-graphene)

RESULTS AND DISCUSSION

Isolation and characterization of Diatom Silica

The three diatom samples were cleaned by removing the organic components present in diatoms. The original diatom cell suspension was brownish in color and upon the addition of concentrated H_2SO_4, it turned into green. Excess amount of H_2SO_4 made the diatom suspension into grayish white indicating that the organic components have been removed (Jeffryes et al. 2007). Scanning electron microscopy (SEM) gave a magnified view of the architecture of the diatom species being studied. Acid oxidation with concentrated sulfuric acid removed the organic matter from the frustules or the cell walls of the biosilica rendering the cell walls of the species to be porous. SEM images of the diatom samples in Figure 2 revealed a unique and intricate design of the frustules. Figures 2a-2c is a summary of the structure and organization of the porous layers of the silica frustules of (a) *Amphora sp*., (b) *Navicula ramossisima*, and (c) *Skeletonema sp*.

These observations indicate the shape of each species. Figures 2a and 2b, *Amphora sp*. and *Navicula ramossisira*, respectively, are elongated like a pen, so they are classified as pennate. *Skeletonema sp*. in Figure 2c is considered as centric diatom. From the SEM images, the lateral size of the diatom can be estimated as 6 – 8 microns.

To confirm that silica was isolated from diatom cells, FTIR analysis was done in the 4000-500 cm^{-1} range. IR spectra in Figure 3 show that siloxane and silanol groups are present. The main absorption bands for diatom silica as depicted in Figure 3A were found at 3500, 1128, 820 and 479 cm^{-1}. The band at 3500 cm^{-1} is due to free silanol group (SiO-H) and the band at 1128 cm^{-1} represents the siloxane (Si-O-Si) group stretching. Figure 3B is zoomed in at the Si-O stretching of silanol group and bending vibration of siloxane with absorption peaks at 820 and 479 cm^{-1}, respectively (Khraisheh et al. 2005).

The Brunauer–Emmet–Teller (BET) surface area of the diatom silica was calculated using the N_2 adsorption/desorption isotherms in Figure 4. The calculated values are 11 m^2/g, 4 m^2/g and 2 m^2/g for *Amphora sp., Navicula ramossisira* and *Skeletonema sp*., respectively. The surface area for diatoms differs among species. This could be attributed to an incomplete acid oxidation of the organic coating. This organic matrix also varies within species and they were found to be difficult to remove. If they are not burned off completely, then the remaining organic coating could not expose fully all the silica pores. This will lead to a decrease in the surface area (Chen et al. 2010). The IR spectra of the three diatoms in Figure 3A confirms presence of some organics as shown in peak 1 (1700 cm^{-1}) for C=O and peak 2 (1400-1600 cm^{-1}) for aromatic carbon. It is also evident that the *Skeletonema sp.* diatom has the aromatic peak aside from the C=O band. This could explain the very low specific surface area of this species.

The XRD pattern of diatom silica in Figure 5 suggests that diatom silica is amorphous with angle of diffractions ranging from $2\Theta = 20^\circ$ - 26° (Kaufhold et al. 2008). The structure of diatom, therefore, may be considered as a random network of tetrahedrally bound silicon atoms. This corresponds to a poorly ordered silica (Kamatanil 1971). Other XRD peaks at $2\Theta > 26^\circ$ may indicate that the diatom silica also consists a little amount of quartz and cristobalite silica (Wang 2002).

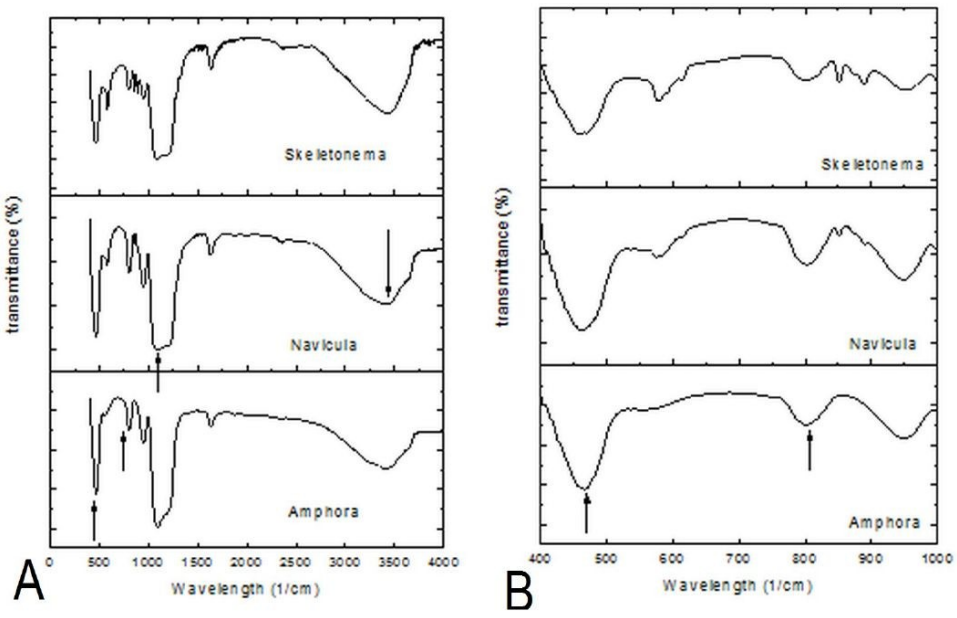

Figure 3. FTIR spectra of cleaned diatom silica: (A) wide view and (B) zoomed in at the region of SiO2 vibrational frequencies.

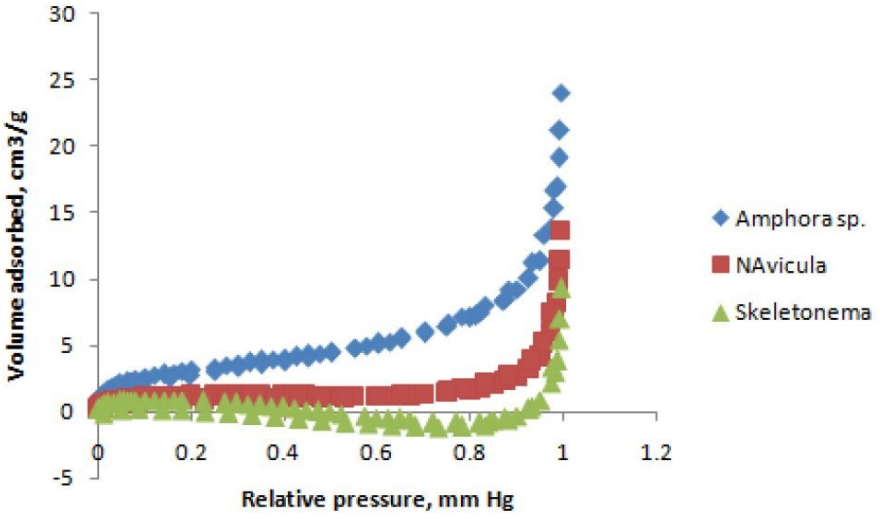

Figure 4. N2 adsorption/desorption isotherms of diatom silica.

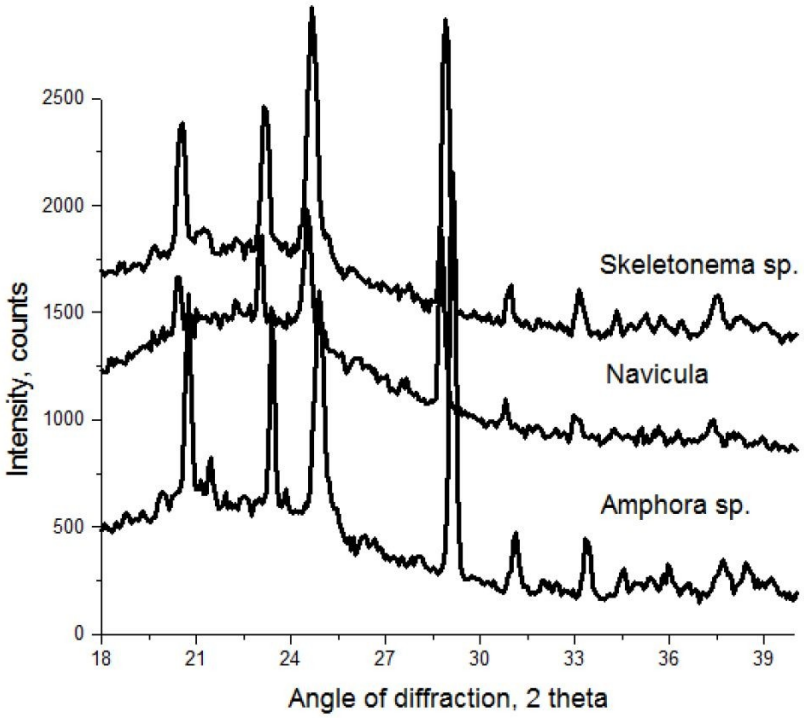

Figure 5. XRD pattern of diatom silica showing its amorphous peak at 2Θ range of 20˚- 26˚.

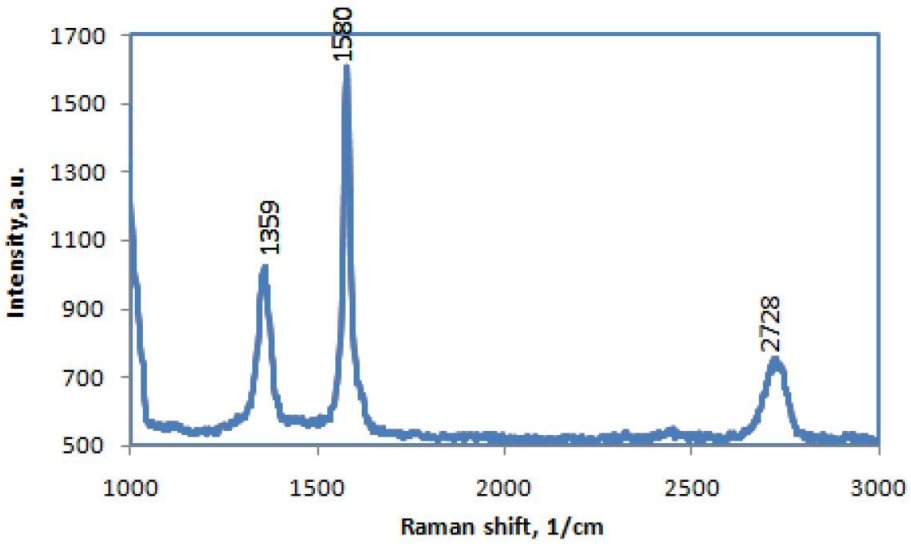

Figure 6. Raman spectrum of graphene prepared by liquid exfoliation using NMP as solvent.

Synthesis and characterization of graphene

Raman spectroscopy is an important tool in the analysis of graphite-like materials such as graphene and carbon nanotubes. Their strong Raman response is due to resonant enhancement by C-C π states. The "quality" of graphite-like samples is often studied through analysis of the "D" peak at around 1300 cm^{-1} which is due to breathing modes in C-C ring structures and whose presence is indicative of defects and the "G" peak at around 1600 cm^{-1}, which is due to C (sp^2)-C-(sp^2) bond stretching vibrations. The "2D" peak at around 2700 cm^{-1} ascribes to the out-of-plane vibration mode and its shape has been used to determine the number of layers in a multi-layer graphene. Figure 6 shows the Raman spectra of exfoliated graphene with three major peaks, the D, G and 2D. The presence of the D band suggests the occurrence of few defects in the exfoliated graphene. The 2D band implies the presence of several layers of exfoliated graphene (Das et al. 2008).

The AFM topography image in Figure 7 shows a bit of "shadowing" but reveals what appears to be agglomerated graphene flakes cast on silicon surface. The Z-height of a sample imaged was estimated to be about 15 nm. This corresponds to several graphene layers (a single layer has reported heights ranging from 0.3 to 1 nm from AFM studies). The large thickness may be agglomeration due to solvent evaporation and manner of sample preparation for AFM imaging. (Englert et al. 2011).

Prepared stock graphene and diluted graphene were subjected to UV-Vis analysis for a wavelength scan of 200 nm to 700 nm. Spectra in Figure 8 revealed a characteristic shoulder peak at λ = 270 nm for all graphene suspensions which is due to $\pi - \pi^*$ electronic conjugation. This peak has been reported for graphene in aqueous solvent (Li et al. 2008). The spectra

absorbance peak intensity diminishes as the graphene dispersion is diluted. Twenty times dilution of stock graphene gave a very low absorbance peak while the stock graphene (undiluted) has the highest absorbance.

Graphene-Diatom Silica Synthesis and Characterization

Upon 24 h equilibration of 5-mL graphene suspensions with 1 mg bio-silica, it was observed that different diatom species showed varying adsorption behavior (Figure 9). *Navicula ramossisira* and *Skeletonema sp*. revealed a clear supernatant liquid and a black precipitate. Both species did not clarify quickly after the addition of graphene solution. *Skeletonema sp*. took about 30 min to have a clear solution while *Navicula ramossisira* had a clear solution after 24 hrs. This observed behavior indicates that no flocculation has occurred. *Amphora sp*.-graphene gave a black supernatant liquid and a black precipitate after 24-hr equilibration.

Thermogravimetric analysis (TGA) of diatom silica- graphene revealed the total amount of graphene present in 0.100 mL of graphene dispersion. A slight change in mass was observed at 600 ˚C when the system was under air flow with oxygen present. Combustion of adsorbed and non-adsorbed graphene could have occurred from this temperature until 800˚C. At the end of the run, the platinum pan contained a white solid substance which was that of diatom silica and there was no visible of grayish graphene. This is another evidence of the presence of graphene in diatom silica. All of the graphene could have combusted during the process. This can be inferred in the change in mass in the TGA curve. From the TGA curves, the total masses of graphene per 0.100 mL of graphene suspension were determined to be 0.0306 mg, 0.0449 mg and 0.0188 mg for the diatom species *Amphora sp., Navicula ramossisira* and *Skeletonema sp*., respectively.

To investigate the electronic property of the composite, electron mobility was measured by the Hall equipment. The Hall mobility was determined from the sheet resistance and sheet carrier density that the instrument calculated. The average mobilities were 3.2 x 10^1, 9.3 x 10^2 and 1.2 x 10^2 cm^2/V.s for graphene-*Amphora*, graphene-*Navicula* and graphene-*Skeletonema*, respectively. The observed mobilities can be attributed to the presence of graphene in the composite because diatom silica alone will not exhibit any electron mobility. The magnitude of the electron mobility does not necessarily follow the trend in the total graphene in diatom silica. This is because the amount of sample that was drop-casted in a 10.0 mm x 10.0 mm substrate does not represent the total graphene in diatom.

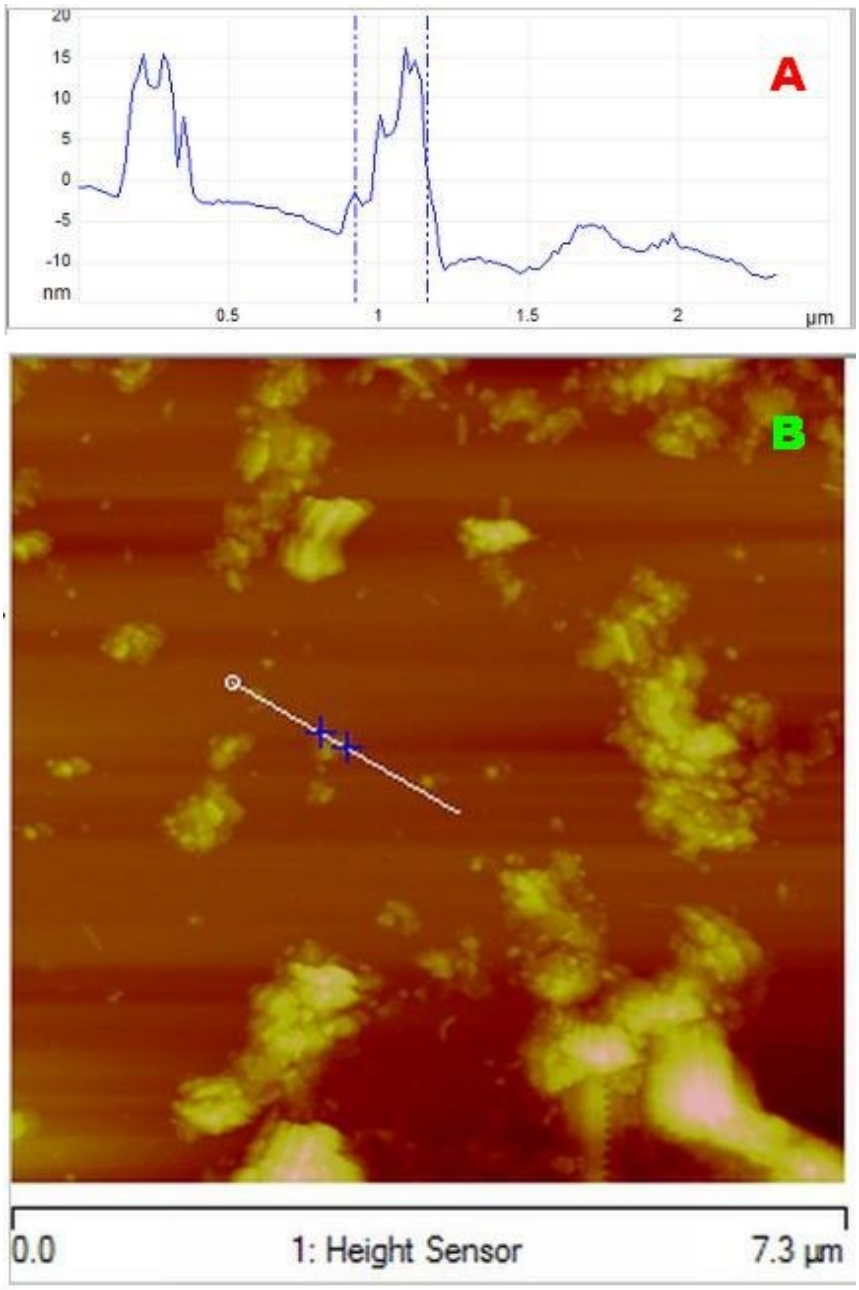

Figure 7. (A) AFM image and (B) height profile of graphene prepared by liquid exfoliation.

Figure 10 shows the Raman spectra of graphene and graphene-diatom silica. Three major peaks can be observed in the spectra: D (1350 cm^{-1}) band, G band (1585 cm^{-1}) and a 2D (2700 cm^{-1}) band. The Raman spectra of graphene-diatom showed a shift of the D, G and 2D bands to a lower frequency (red-shifted) compared with that of pristine graphene. Other groups have reported similar results of G peak red shifting after thermal and chemical reduction of GO. This observation is due to the local disorder band induced by the reduction process. In the case of graphene-diatom, the shift to a lower frequency is possibly due to the noncovalent interaction between graphene and diatom silica (Cuong et al. 2010). The interaction of diatom silica with graphene varies among the 3 species as observed in the way the band intensity changes. Graphene-Sk showed a much more pronounced D and G band than the other composites. The shape and architecture of *Sketonema sp.*, which is very different from *Amphora* and *Navicula,* could have dictated its interaction with grapheme.

From the SEM data, it can be concluded that graphene was not inserted into the pores of the diatom in the course of the adsorption process. Although there was no significant electronic bonding interaction between graphene and diatom silica as illustrated in the IR peaks, the images suggest that only physisorption by van der Waals interaction occurred between graphene and the diatom silica. A theoretical study was done by Wojdel *et al*. to calculate for the binding energy of CNT and silica. Their results revealed that the binding energy for CNT and silica implied for a typical physisorption interaction. The attraction of the π electrons towards the inner oxygen atoms led to the depletion of the σ system around the CNT so that electrons were slightly delocalized toward the silica rings. This was responsible for the noncovalent interaction between CNT and silica (Wojdel et al. 2005). These findings could also explain the interaction between graphene and diatom silica during the adsorption process since graphene and CNT have the same π-π electronic conjugation. This adsorption location of graphene on the silica is illustrated by black particles in the periphery of the diatom as shown in Figures 2D-2F.

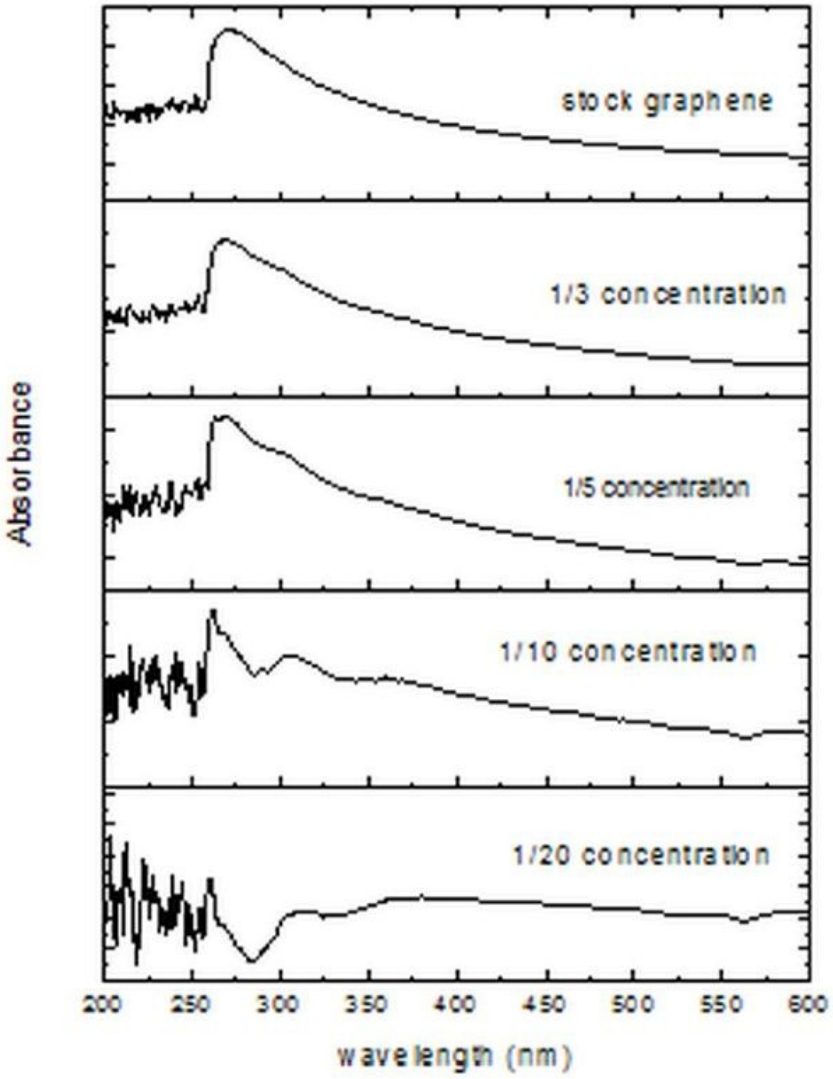

Figure 8. Absorbance of graphene at different concentration.

CONCLUSION

The synthesis and characterization of graphene-diatom silica composite were demonstrated in this work. Raman spectroscopy of the graphene-diatom silica materials revealed band shifts in the D, G and 2D peaks which are indicative that there is an interaction between graphene and diatom silica. Through thermogravimetric measurements and UV-Vis analyses, the amounts of graphene in the diatom species were 0.306 mg/mL, 0.449 mg/mL and 0.188 mg/mL for *Amphora sp., Navicula ramossisira* and *Skeletonema sp*., respectively. Hall mobility and SEM of the graphene-diatom also illustrate presence of graphene on diatom silica. The results and insights presented in this study are positive indications that advanced inorganic hybrids such graphene and diatom silica can be possibly synthesized. The possible applications of graphene-diatom silica in environment and energy are currently being studied by the authors.

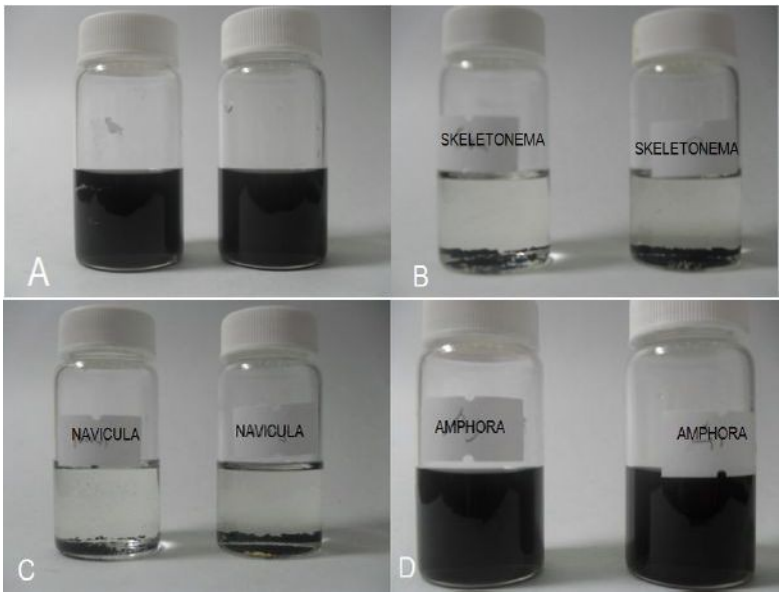

Figure 9. Graphene and diatom silica (A) before 24 hrs equilibration; (B-D) after 24 hrs equilibration; B-*Skeletonema*, C-*Navicula*, D-*Amphora.*

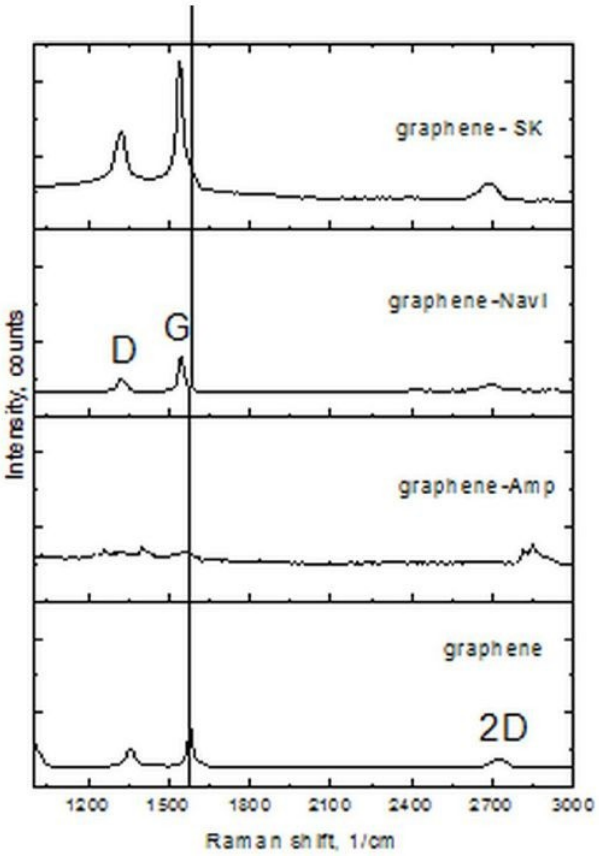

Figure 10. Raman spectra of graphene and graphene-diatom silica

ACKNOWLEDGEMENT

The authors would like to acknowledge the Commission on Higher Education (CHED) for financial support , the Research Center for Applied Sciences (RCAS) of Academia Sinica, Taiwan for AFM, Raman and Hall measurements, the Department of Chemistry of Michigan State University, East Lansing, Michigan, USA for XRD and BET surface area measurements, the Department of Materials Science of Ateneo de Manila University for acquiring the SEM images and Southeast Asian Fisheries Development Center Aquaculture department (SEAFDEC-AQD), Tigbauan, Iloilo City for the diatom samples.

CONFLICT OF INTEREST

The authors declare no conflict of interest.

CONTRIBUTION OF AUTHORS

Dr Erwin P Enriquez: Contributed in the conceptualization, design of the study and supervision of the conduct of experiments at the Ateneo de Manila, in the data analysis, and editing of the manuscript.

Ms. Juliet Q Dalagan: Contributed in the design and conceptualization of the experiments, implemented all the experiments, data analysis, and the primary writing of the manuscript.

REFERENCES

Allen M, Tung V, Kaner R. Honeycomb Carbon: A Review of Graphene. Chem. Rev 2010; 110: 132–145

Bismuto A , Setaro A , Maddalena P , De Stefano l , De Stefano M. Marine diatoms as optical chemical sensors: A time-resolved study. Sensors and Actuators B 2008; 130: 396–399

Chen S, Zhu J, Wu X, Han Q, Wang X. Graphene Oxide-MnO_2 Nanocomposites for Supercapacitors. ACS Nano 2010; 4 (5): 2822–2830

Chu YH, Yamagishi M , Wang ZM, Kanoh H, Hirotsu T. Synthesis of Nanoporous Graphite-Derived Carbon-Silica Composites by a Mechanochemical Intercalation Approach. Langmuir 2005; 21: 2545-2551

Chu YH, Yamagishi M, Wang ZM, Kanoh H, Hirotsu T. Adsorption characteristics of nanoporous carbon–silica composites synthesized from graphite oxide by a mechanochemical intercalation method . Journal of Colloid and Interface Science 2007; 312: 186–192

Cooksey B, Cooksey K. Use of fluorophore-conjugated lectins to study cell-cell interactions in model marine biofilms. Applied and Environmental Microbiology 2005; 71(1):428-35.

Cuong TV, Pham VH, Tran QT, Hahn SH, Chung JS, Shin EW, Kim EJ. Photoluminescence and Raman studies of graphene thin films prepared by reduction of graphene oxide. Materials letters. 2010; 64: 399-401

Das A, Chakraborty B, Sood AK. Raman spectroscopy of graphene on different substrates and influence of defects. Bull. Mater. Sci. 2008; 31: 3, 579–584.

De Stefano L., Rotiroti L, De Stefano M, Lamberti A, Lettieri S., Setaro A, Maddalena P. Marine diatoms as optical biosensors Biosensors and Bioelectronics. 2009, 24, 1580–1584

Englert JM, Dotzer C, Yang G, Schmid M, Papp C, Gottfried JM, Steinrück HP, Spiecker E, Hauke F, Hirsch A. Covalent bulk functionalization of graphene. Nature Chemistry 2011; 3: 279–286

Grzelczak M, Correa-Duarte m, Liz-Marz l. Carbon Nanotubes Encapsulated in Wormlike Hollow Silica Shells. Small 2006; 2: 10, 1174 – 1177

Hernandez Y, Nicolosi V, Lotya M, Blighe F, De S ,McGovern IT, Holland B, Byrne M, Sun Z, Yurii K. Gun'KO, Boland JJ, Niraj P, Duesberg G, Krishnamurthy S, Goodhue R, Hutchison J, Coleman JN, Scardaci V, Ferrari AC. High-yield production of graphene by liquid-phase exfoliation of graphite. Nature Nanotechnology 2008; 3: 9, 563-568

Hubert T, Shimamura A, Klyszcz A. Carbon–silica sol-gel derived nanomaterials. Materials Science-Poland 2005; 23: 1, 61-68

Jeffryes C , Gutu T, Jiao J, Rorrer G . Two-stage photobioreactor process for the metabolic insertion of nanostructured germanium into the silica microstructure of the diatom *Pinnularia* sp. Mater Sci Eng C 2008; 28, 1, 107

Kamatani I A. Physical and chemical characteristics of biogenous silica . Marine Biology, 1971; 8: 89-95

Kawashima D, Aihara T, Kobayashi Y, Kyotani T, Tomita A. Preparation of Mesoporous carbon from Organic Polymer/Silica Nanocomposite . J. Chem. Mater. 2000; 12: 3397-3401

Kaufhold S, Dohrmann R, Ulrichs Ch. Shelf life stability of diatomites.Applied Clay Science. 20008; 41:158–164

Khraisheh MAM, Al-Ghouti MA , Allen SJ , Ahmad MN. Effect of OH and silanol groups in the removal of dyes from aqueous solution using diatomite. Water Research 2005; 39: 922–932

Li D, Muller MB, Gilje S, Kaner RB, Wallace GG . Processable aqueous dispersions of graphene nanosheets, Nature Nanotechnology 2008; 3: 101-105.

Soldano C, Mahmood A, Dujardin E. Production, properties and potential of graphene. Carbon 2010; 48: 2127-2150

Song L, Fredin N, Feng D, Campbell CG, Lee HJ, Gu D, Jones RL, Forster AM, Zhao D, Yager KG, Vogt BD. Robust conductive mesoporous carbon–silica composite films with highly ordered and oriented orthorhombic structures from triblock-copolymer template co-assembly. J. Mater. Chem 2010; 20: 1691–1701

Spaulding S, Edlund M. Skeletonema. In: Gallagher JC, ed. Population genetics of *Skeletonema costatum*(Bacillariophyceae) in Narragansett Bay. Journal of Phycology, 1980; 16, 464-474.

Vrieling EG, Beelen TPM, Van Santen RA, Gieskes WWC. Diatom silicon biomineralization as an inspirational source of new approaches to silica production. Journal of Biotechnology 1999; 70: 39–51

Wan Y, Min YL, Yu SH. Synthesis of Silica/Carbon-Encapsulated Core-Shell Spheres: Templates for Other Unique Core-Shell Structures and Applications in in Situ Loading of Noble-Metal Nanoparticles. Langmuir 2008; 24: 5024-5028

Wang D, Hu D, Kou R, Zhang J, Choi D, Graff GL, Yang Z, Liu J, Nie Z, Pope MA, Li J, Saraf LV, Aksay IA. Ternary Self-Assembly of Ordered Metal Oxide_Graphene Nanocomposites for Electrochemical Energy Storage. ACS Nano, , 2010; 4: 3, 1587–1595

Wang Y, Tang Y, Dong A, Wang X, Ren N, Gao Z, Zeolitization of diatomite to prepare hierarchical porous zeolite materials through a vapor-phase transport process. J. Mater. Chem., 2002, 12, 1812–1818

Wang Z, Shishibori K, Hoshinoo K, Kanoh H, Hirotsu T. Examination of synthesis conditions for graphite-derived nanoporous carbon–silica composites. Carbon 2006; 44: 2479–2488

Watcharotone S,Jung I, Chen SF, Dikin DA, Dommett GHB, Liu CP, Stankovich S, Evmenenko G, Nguyen ST, Piner R, Wu S,Ruoff RS. Graphene-Silica Composite Thin Films as Transparent Conductors. Nano Lett. 2007; 7: 7, 1888-1892

Wojdel JC, Bromley ST. Interaction of SiO_2 with Single-Walled Carbon Nanotubes. J. Phys. Chem. B 2005; 109: 4, 1387-1391

Yu H, Fugetsu B. A novel adsorbent obtained by inserting carbon nanotubes into cavities of diatomite and applications for organic dye elimination from contaminated water. Journal of Hazardous Materials 2010; 177: 138–145